Drain Water Heat Recovery Storage-type Unit for Residential Housing

Torras S., Oliet C., Rigola J., Oliva A.*

Heat and Mass Transfer Technological Center (CTTC), Universitat Politècnica de Catalunya-BarcelonaTech (UPC)
ESEIAAT, Carrer Colom 11, 08222, Terrassa (Barcelona), Spain
[1,2,3,4]cttc@cttc.upc.edu

Abstract

The drain water heat recovery (DWHR) system is an interesting household technology to reduce energy costs and environmental impact. The objective of the utilization of these devices is the recovery of the waste heat from domestic warm drain water, and transferring it to cold water entering the house. A drain water heat recovery unit has been built in this work. The authors are using both numerical and experimental tools to design and study the performance of this device, focusing on the analysis of a specific drain water heat recovery storage-type based on a cylindrical tank with an internal coiled pipe. The numerical simulation has been performed using an in-house platform, where the different elements of the DWHR storage are linked to solve the system. On the other hand, an experimental infrastructure has been developed to analyse of the system, which has been instrumented to provide detailed information of its heat recovery and storage capacities and temperature map. Different internal flow rates and operational temperatures have been studied. From the results obtained it can be said that the device shows interesting heat recovery and storage capacities, while the numerical platform shows promising comparison results against the experiments.

Keywords: drain water; heat recovery; sensible heat storage; accumulation water tank; CFD; experimental

*Corresponding author. Tel.:+34-93-739-8192; Fax:+34-93-739-8101
Email address: cttc@cttc.upc.edu (Oliva A.)
URL: http://www.cttc.upc.edu (Oliva A.)

1. Introduction

Developing efficient and inexpensive energy recovery devices is as important as developing new energy sources. Heat is necessary for many building applications and, therefore, must be generated, stored and used efficiently to take advantage both economically and environmentally. The drain water heat recovery (DWHR) is designed to recover the residual energy from the hot or warm drain water, and this recover energy is used to preheat the incoming cold water. This interesting technology is an efficient and low-cost way of recovering thermal energy for its reutilization in typical building processes, as space heating and sanitary hot water generation. The residential sector accounts for 26% of the total consumption in USA. Of this, 37% is electricity for lighting, cooling, and appliances. The remaining energy used is attributed to heating: 45% for space heating and 18% for water heating [1]. Therefore, residential water heating accounts for 4% of the total national energy demand. In other countries like the UK, the residential sector representing a 29% of total energy consumption in the country. Of this, 65% for space heating and 16% for water heating [2]. Thus, the energy used for heating water represents a significant part of the total energy which is consumed in a typical household. There are many works, i.e. Boait et al. [3] and Leidl et al. [4], where different technologies are analysed in order to save energy used to heat domestic water, including solar water heating (SWH), gas boilers, heat pumps, an immersion heater and drain water heat recovery.

There are different types of DWHR systems. Authors like Cooperman et al. [5] classified into two types: on-demand and storage. For the on-demand type, the warm drain water flows down in the inner pipe while simultaneously the incoming cold water flows up in the external coiled tube. This type of DWHR is referred to as a gravity film heat exchanger, see Fig. 1 (left). In the storage type described by Cooperman, the warm drain water flows through the heat exchanger heating the clean water into the tank for future use. Fig. 1 (right) shows the storage type used in the current work, this configuration is inverted with respect to the configuration described above, the warm drain water is into the tank and the clean water flows through the heat exchanger.

In the literature there are some studies on the DWHR systems, most of them of the falling film heat exchanger, also known as a vertical inline drain water heat recovery heat exchanger. Zaloum et al. [6] demonstrated that the use of vertical exchanger is justified when the movement of the two media

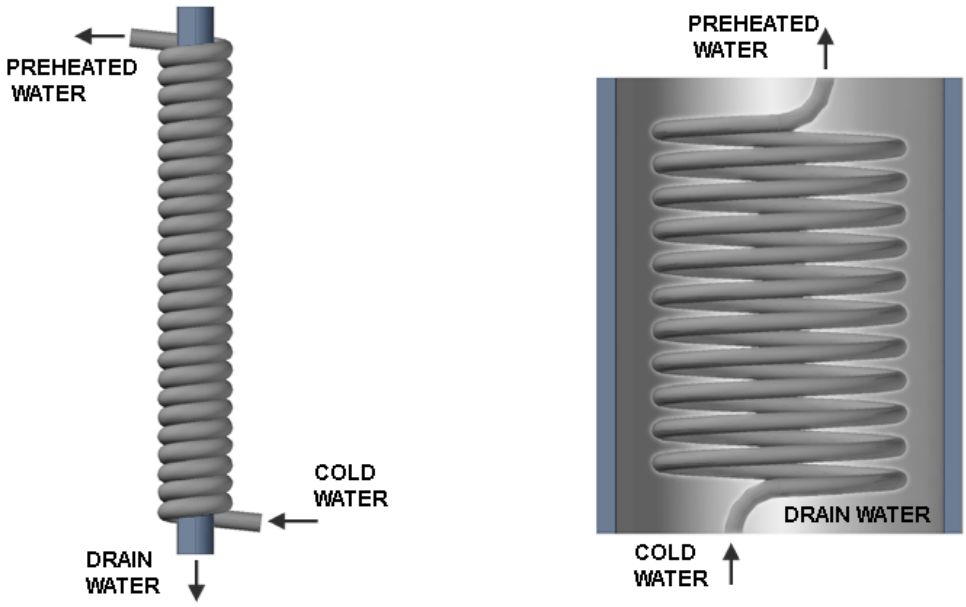

Figure 1: On the left, on-demand DWHR. On the right, storage DWHR.

is simultaneous. They conducted their experiments on eight different film exchangers to determine the effect of flow rate, temperature and configuration in heat recovery performance. In the different film exchangers, the maximum heat recovered is reached at the lowest flow rates (using the same flow rates for the two media), while the other parameters showed no significant effect on the heat recovery efficiency. McNabola et al. [7] and Wong et al. [8] analysed the efficiency of using the DWHR in a horizontal position. Both authors used a simple single-pass counter-flow heat exchanger installed horizontally beneath the shower drain.

In works [9, 10] the DWHR are introduced in heat pump systems, where numerical models have been developed to their analysis. Wallin et al. [11] studied experimentally the performance of this type of device in a heat pump system. In their work, the exchanger had the capacity to recover more than 25% of the energy available in the drain water for the investigated flow rates (as an evaporator to recover waste heat from shower water).

Ni et al. [12] analysed the potential saving of incorporating a DWHR in heat pump system to reclaim heat from residential wasterwater for space heating, space cooling and domestic water heating. A numerical model has been developed for the comparison of annual energy consumption and drink-

ing water savings between the water energy-recovery system and the conventional building energy system. In that study, the drain water heat recovery has a similar configuration to the current work.

Heat exchangers with coiled pipe are used in many applications such as the nuclear industry, refrigeration, food industry, etc. And this is because the coiled pipe has higher heat transfer coefficients in comparison with a straight tube [13], while it also allows a more compact structure. The modification of the flow in the coiled pipe is due to the centrifugal forces, where the curvature of the tube produces a secondary flow field with a circulatory movement (Dean [14, 15]).

There is a considerable amount of work focused on the internal heat transfer in coiled pipe. Works carried out since the end of the decade of the 50s have generated interesting correlations based on experimental data, such as Ito [16], Seban et al. [17], Rogers et al. [18], Schmidt [19] and Gnielinski [20]. These correlations have been widely used for the internal heat transfer in coiled pipe. Numerical investigation were performed to understand the heat transfer in laminar flow in coiled pipes by Dravid et al. [22]

However, little is known about the external heat transfer in coiled pipe. Ali conducted experimental studies for coiled pipes immersed in water [23] and glycerol-water [24]. From his studies, Ali developed a correlation to evaluate the outside heat transfer. Xin and Ebadian [25] conducted experimental investigations of the outside heat transfer for natural convection from coiled pipes in air. Subsequently, they investigated the effect of the Prandtl number and geometrical parameters on the outside heat transfer from the coiled pipes immersed in air, water and ethylene-glycol [26].

A similar configuration to the current work, but used in another type of applications, can be seen in other works such as Prabhanjan et al. [27] and Fernández-Seara et al. [28]. They worked with coiled pipes immersed in water and the fluid inside the coiled pipe was water. In addition these authors combine experimental and numerical study. Prabhanjan et al. developed a model to predict the outlet temperature of a fluid flowing through a helically coiled heat exchanger. Fernández-Seara et al. developed a numerical model in order to predict the heat transfer process and pressure drop in a helically coiled heat exchanger. In the two works described above the numerical resolution is carried out for the fluid flow through the coiled pipe with a simplified external condition to take into account the heat transfer between the fluid flow and the fluid inside the tank. In those works the fluid inside the tank is not simulated, instead a constant temperature for that fluid is defined. In

the present study the whole fluid inside the tank is solved in three dimensions (3D) and considering transient state. This feature is critical to study the evolution of the fluid temperature inside the tank which is essential to calculate the heat recovery performance of the device. Therefore, the present model allows to have a greater insight of such systems.

In this paper, the transient evolution of the DWHR storage system is studied in order to determine its performance. For this reason in this research, the authors are developing both numerical and experimental tools to design and study the performance of this kind of systems.The numerical simulation has been performed using the in-house multi-level platform that links three codes to solve the system (in-tank + tube + in-tube). On the other hand, an experimental infrastructure has been developed for the analysis of the system, which has been instrumented to provide detailed information of heat recovery from the waste water, heat storage capacity and temperature map. Both numerical and experimental results presented in the paper show the potential of the proposed methodology as a very useful tool to obtain the performance of drain water heat recovery device through the parametrization of the geometric variables and operating conditions when designing a DWHR storage device. The drain water used in the DWHR storage device arises from domestic washing operations (especially washing machines, but also other sources, such as baths, showers, hand basins and kitchen sinks), but specifically exclude foul or black water sources.

2. Numerical Model

In this work the proposed numerical resolution is based on solving at different scales (Lopez et al. [29]) using the in-house NEST thermal systems simulation platform (Damle et al. [30]), which allows the linking between the three different elements (fluid inside tank, tube and in-tube fluid), constituting the DWHR storage system under study. Each of these elements can be solved independently and using different levels of modelling (from global to fully three-dimensional models), while at the same time they are linked to each other through their boundary conditions. An in-house CFD&HT (Computational Fluid Dynamics & Heat Transfer) software, called TermoFluids (Lehmkuhl et al. [31]), is used for solving the fluid movement inside the tank (section 2.1), while the tube is discretised in a two dimensional way and the in-tube flow is solved considering a single-phase fully-implicit one-dimensional model (section 2.2), where the governing equations (momentum,

continuity, and energy) are discretised along the whole coil domain (Morales-Ruiz et al. [32]). After that, the coupled resolution between the different elements that composed the system is explained in section 2.3.

2.1. Numerical Simulation of In-Tank Free Convection

TermoFluids software uses efficient algorithms, which compute in parallel adapting the solving strategy to the hardware architecture (communication, memory distribution,) [31]. The Navier-Stokes equations (1)-(3) are applied to the control volumes of the domain and converted into algebraic ones using three-dimensional unstructured collocated meshes, symmetry-preserving formulation, and considering Boussinesq assumption.

$$\mathbf{M}\mathbf{u} = 0 \tag{1}$$

$$\rho\Omega\frac{\partial \mathbf{u}}{\partial t} + \rho\mathbf{C}(\mathbf{u})\mathbf{u} = \mathbf{D}((\mu + \mu_t)\mathbf{u}) - \Omega\mathbf{G}p + \rho\vec{g}\beta(T - T_0) \tag{2}$$

$$\Omega\rho c_p\frac{\partial \mathbf{T}}{\partial t} + \rho c_p\mathbf{C}(\mathbf{u})\mathbf{T} + \mathbf{D}\left((\lambda + \lambda_t)\mathbf{T}\right) = 0 \tag{3}$$

where $\mathbf{u} \in \mathrm{R}^{3\mathrm{N}}$, $p \in \mathrm{R}^{\mathrm{N}}$ and $\mathbf{T} \in \mathrm{R}^{\mathrm{N}}$ are the velocity vector, pressure and temperature, respectively (here N applies for the total number of control volumes (CV) of the discretised domain), μ is the dynamic viscosity, λ is the conductivity, ρ is the density, and c_p is the specific heat. The μ_t is turbulent dynamic viscosity and λ_t is the turbulent conductivity, obtained by applying the turbulent model. Convective and diffusive operators in the momentum equation for the velocity field are given by $\mathbf{C}(\mathbf{u})=(\mathbf{u}\cdot\nabla) \in \mathrm{R}^{3\mathrm{Nx3N}}$, and $\mathbf{D} = \nabla^2 \in \mathrm{R}^{3\mathrm{Nx3N}}$, respectively. Gradient and divergence operators are given by $\mathbf{G}=\nabla \in \mathrm{R}^{3\mathrm{NxN}}$ and $\mathbf{M}=\nabla \in \mathrm{R}^{\mathrm{Nx3N}}$, respectively. $\Omega \in \mathrm{R}^{\mathrm{N}}$ is a matrix with the volumes of the cells.

For the temporal discretisation of the momentum equation, a fully explicit second-order Adams-Bashford (AB2) scheme has been used for the convective and the diffusive terms, while for the pressure-gradient term an implicit first-order scheme has been employed. The Courant-Friedrichs-Lewy (CFL) condition is used to determine the time step, in order to ensure convergence/numerical stability requirement for the explicit scheme. To solve the velocity-pressure coupling, a classical fractional-step method is used [33, 34].

The governing equations are discretised on a collocated unstructured grid arrangement by means of second-order conservative schemes [35]. Such discretisation preserves the symmetry properties of the continuous differential operators, i.e., the conservation properties are held if the convective term is discretised by a skew-symmetric operator, and the diffusive term is approximated by a symmetric, positive-definite coefficient matrix.

LES modelling has been adopted in this paper to handle turbulence, in order to reduce computational resources compared to Direct Numerical Simulation (DNS) approach, and allowing an unsteady computation unlike RANS (Reynolds Averaged Navier Stokes) by space filtering. In this simulation, a VMS (Variational Multiscale) model has been selected. The VMS model was originally formulated for the Smagorinsky model by Hughes [36] in the Fourier space, and has given very accurate results in previous works [37, 38, 39]. In VMS three classes of scales are considered: large, small and unresolved scales. The first two classes are solved with LES-WALE (Large Eddy Simulation Wall-Adapting Local Eddy-viscosity), whereas the unresolved scales are modelled.

2.2. Numerical Simulation of In-Tube Single-Phase Flow

The numerical simulation model of the thermal and fluid dynamic behaviour of single-phase flow inside ducts is obtained from the integration of the fluid conservation equations (momentum, continuity and energy) in a one-dimensional way along the tube domain over a finite control volume as shown in Fig. 2. Considering that the transient term is evaluated using the first-order approximation ($\partial\phi/\partial t \approx (\phi - \phi^0)/\Delta t$) and that the control volume values are obtained from an arithmetic mean between the inlet w and outlet e faces ($\bar{\phi} \approx (\phi_e - \phi_w)/2$), the semi-discretised governing equations show the following form:

$$\frac{\partial \bar{m}}{\partial t} + \dot{m}_e - \dot{m}_w = 0 \tag{4}$$

$$\frac{\partial(\bar{m}\bar{v})}{\partial t} + \dot{m}_e v_e - \dot{m}_w v_w = (p_w - p_e)S - \bar{\tau}\pi\, d_i \Delta z - mgsin\theta \tag{5}$$

$$\frac{\partial \bar{m}(\bar{h} + \bar{e}_c + \bar{e}_p)}{\partial t} + \dot{m}_e(\bar{h} + \bar{e}_c + \bar{e}_p)_e - \dot{m}_w(\bar{h} + \bar{e}_c + \bar{e}_p)_w = \dot{Q}_{wall} + V\frac{\partial p}{\partial t} \tag{6}$$

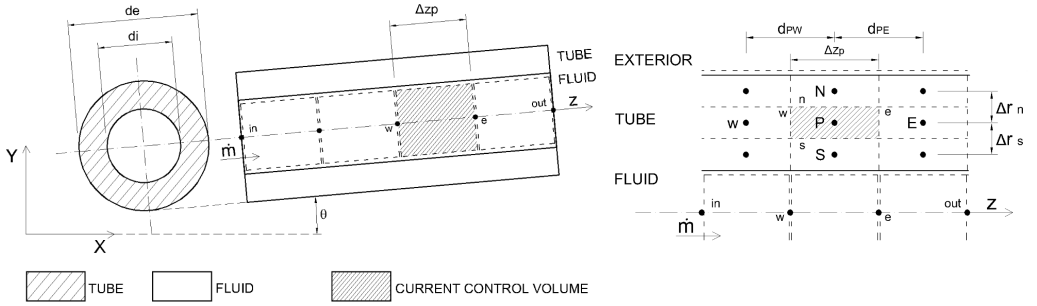

Figure 2: Fluid flow and tube discretisation.

This formulation requires the use of empirical correlations to evaluate two specific parameters: the shear stress (usually calculated from a friction factor, $\bar{\tau} = (f/4)(\dot{m}^2/2\rho S^2)$), and the convective heat transfer coefficient used to evaluate the heat transferred between the tube and the fluid ($\dot{Q}_{wall} = \alpha\pi d_i \Delta z(T_{wall,P} - \bar{T})$). Several correlations based on experimental data can be found in the literature to obtain the inner convection heat transfer coefficient (α) and the friction factor (f) in coiled pipes [17, 18, 19, 20]. The empirical correlations used in this work are given in section 2.2.1.

The flow is evaluated on the basis of a step-by-step numerical implicit scheme. The resulting governing equations are rearranged and solved. Thus, from the duct flow inlet conditions, namely, pressure, enthalpy and mass flow, each control volume outlet state is calculated sequentially. At each control volume the shear stress and the convective heat transfer coefficient are evaluated by means of appropriate empirical correlations. The tube wall temperature map acts as the boundary condition for the whole internal flow at each iteration. More details of the model are found in Morales-Ruiz et al. [32].

The energy balance over the solid part of the tube is also considered. The tube is discretised in a two dimensional way (Fig. 2) and is evaluated with implicit scheme. The resolution procedure is carried out with a line-by-line method, which combines direct method Tridiagonal matrix algorithm (TDMA) and Gauss-Seidel iteration method. The energy equation applied at each solid control volume is expressed as follows:

$$\rho c_p \frac{\partial T_p}{\partial t} S \Delta z_p = \dot{Q}_w + \dot{Q}_e + \dot{Q}_n + \dot{Q}_s \tag{7}$$

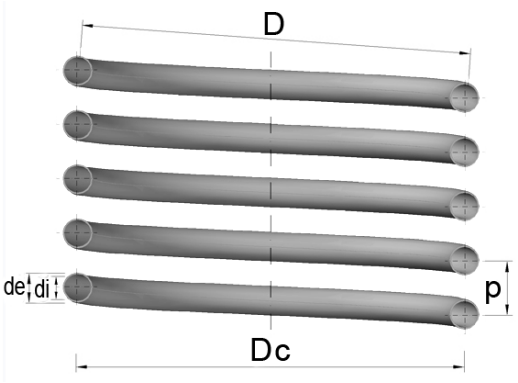

Figure 3: Geometry of a helical coil.

where $\dot{Q}_s$, $\dot{Q}_n$, $\dot{Q}_e$ and $\dot{Q}_w$ are evaluated from the Fourier law (equation 8) for internal nodes.

$$\dot{Q}_i \approx \lambda_i(\frac{T_j - T_P}{d_{Pj}})S_i \tag{8}$$

where i = e, w, n, s and j = E, W, N, S and S_i represents the heat flux cross sectional area.

For the boundary nodes, the balance also takes into account the heat exchanged with the internal or external fluids.

2.2.1. Characteristics of Helical Coil in the DWHR storage system

Fig. 3 gives the schematic diagram of a helical coil. The pipe has inner and outer diameters equal to d_i and d_e, respectively. The coil has a diameter D_c (measured between the projected centres of the pipes), while the distance between two adjacent turns, called pitch, is p.

Gnielinski [20] defines the diameter of curvature of the coil as D, which is obtained from equation (9). Remarkable differences between D and D_c result only for strongly curved tubes and large pitches. For most practical cases, the difference is negligible as p is small compared to D_c. For this reason, many authors do not distinguish between D and D_c.

$$D = D_c\left(1 + \left(\frac{p}{\pi D_c}\right)^2\right) \tag{9}$$

In this work, D is the diameter of curvature used. The relative curvature of the coil is defined as (d_i/D).

Similar to Reynolds number (Re) for flow in pipes, Dean number (De) is frequently used to characterise the flow in a helical pipe. The Reynolds number and the Dean number are defined as,

$$Re = \frac{\rho v d_i}{\mu} \tag{10}$$

$$De = Re\sqrt{\frac{d_i}{D}} \tag{11}$$

The critical Reynolds number for the transition from laminar to turbulent flow in helical coils is a function of the coil parameters. The critical Reynolds number where transition regime begins may be determined using the correlation by Schmidt [21].

$$Re_{cri} = 2300\left[1 + 8.6\left(\frac{d_i}{D}\right)^{0.45}\right] \tag{12}$$

In this work, the inner convection heat transfer coefficient of the water flowing into the coil is determined from the correlation proposed by Gnielinski [20] (equations (13)-(15) for the different flow regimes).

Laminar flow regime:

$$Nu = \left(3.65 + 0.08\left\{1 + 0.8\left(\frac{d_i}{D}\right)^{0.9}\right\} Re^m Pr^{\frac{1}{3}}\right)\left(\frac{Pr}{Pr_{wall}}\right)^{0.14} \tag{13}$$

$$m = 0.5 + 0.2903\left(\frac{d_i}{D}\right)^{0.194} \tag{14}$$

Turbulent flow regime:

$$Nu = \frac{\left(\frac{f}{8} RePr\right)}{1 + 12.7\sqrt{\frac{f}{8}}\left(Pr^{2/3} - 1\right)}\left(\frac{Pr}{Pr_{wall}}\right)^{0.14} \tag{15}$$

The factor $(Pr/Pr_{wall})^{0.14}$ was introduced by Gnielinski into the Schmidt equations [19] to take into account the temperature dependence of the physical properties.

For the transition region $\mathrm{Re}_{cri} < \mathrm{Re} < 22000$, Gnielinski proposes calculated from a linear interpolation of the Nusselt number at Re_{cri} from equation (13) and at $\mathrm{Re} = 22000$ from equation (15).

The friction factor f in the coiled pipe of circular cross-section is calculated by equations (16)- (17) (Gnielinski [40]):

Laminar flow regime:

$$f = \frac{64}{Re}\left(1 + 0.33\left(log_{10}De\right)^4\right)k \tag{16}$$

Transition and turbulent flow regimes:

$$f = \left(\frac{0.3164}{Re^{0.25}} + 0.03\left(\frac{d_i}{D}\right)^{1/2}\right)k \tag{17}$$

Woschni [41] in his experiments observed a decrease of the friction factors with increasing difference between the wall temperature and the mean temperature of the fluid. For this reason a correction factor (k) is introduced using the dynamic viscosity (μ).

$$k = \left(\frac{\mu_{wall}}{\mu}\right)^{0.27} \tag{18}$$

The inner Nusselt number and the friction factor (which are calculated with the above equations) are used to evaluate the shear stress and the heat transferred between the tube and the fluid.

2.3. Coupled resolution

The numerical algorithm takes into account, in a coupled manner, the resolution of the different elements of the system: i) the free convection in the fluid inside the tank (in-tank); ii) the heat conduction through the solid element (coiled pipe); and iii) the fluid flow inside the coiled pipe (in-tube).

Fig. 4 shows the information transfer between domains. In each time step iteration the resolution is carried out in two steps:

- The first one consists on solving the in-tank fluid using the CFD model with the tube temperature map obtained in the previous step.

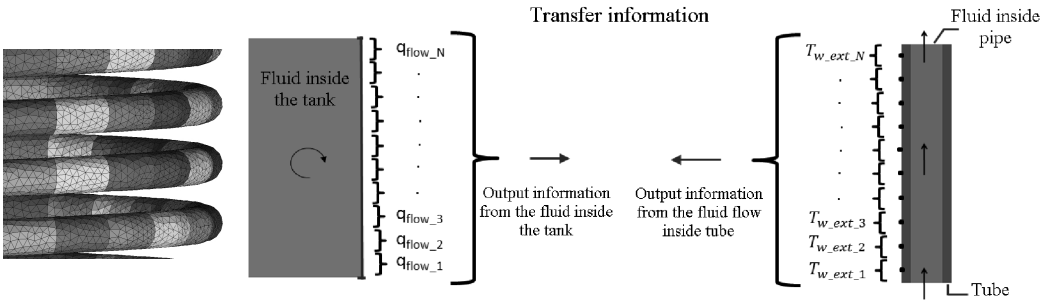

Figure 4: Data exchange between the fluid inside the tank and the wall tube.

- The second step consists of solving the in-tube flow together with the solid part of the tube. The boundary condition for each control volume is the heat flux calculated in the previous iteration from the in-tank fluid. From this process a new temperature map for the tube is obtained.

This implementation has been performed within the NEST platform [30], which allows linking between different elements of the thermal system. The global resolution algorithm used for the resolution of the whole system of elements (comprising for the in-tank fluid, coiled pipe and in-tube fluid) is a Gauss-Seidel method passing through all elements and updating the values. This algorithm has some particularities to facilitate the coupling between parts of the system with different time integration schemes or distinct time steps. The time step of the system is calculated in the in-tank fluid, using the Courant-Friedrichs-Lewy (CFL) condition, as mentioned in section 2.1. In the parallel computing calculation, particularities were used attempting to save computational costs on unnecessary communications between domains and to help the convergence of the in-tube fluid. First, the in-tank fluid domain is forced to work within an internal loop in order to accumulate heat until the sum of in-tank fluid time steps is of the order of one in-tube fluid time step. On the other hand, a specific effort near to the pipe wall in the in-tank mesh has been devoted to assure good coupling of heat transfer between in-tank and in-tube fluids (as explained later in section 4.2).

3. Experimental Setup

An experimental unit has been built to study drain water heat recovery storage systems. The unit provides reliable measurements of their thermal-

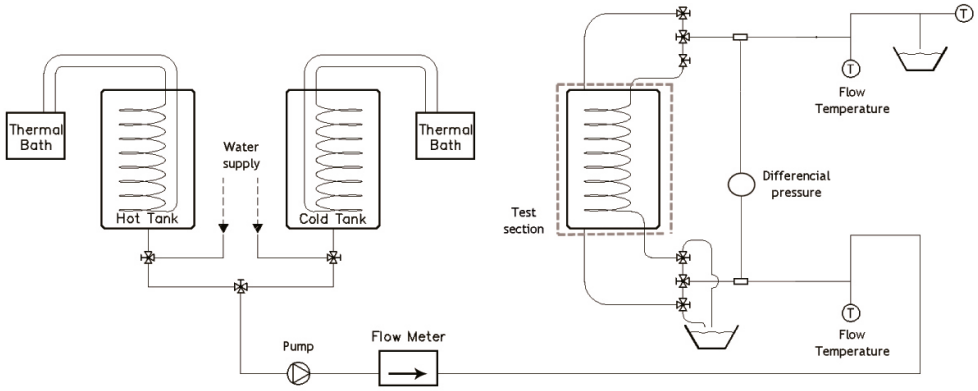

Figure 5: Schematic representation of the experimental unit.

Figure 6: Detailed view of the experimental unit.

hydraulic performance. Furthermore, the experiments were carried out to produce the required data for the boundary conditions definition and results validation of the numerical simulations. The experimental unit is thus designed to supply hot and cold water to a DWHR storage device (test section), and to study its performance accumulating and delivering energy.

Besides the DWHR storage device, the experimental unit is made up of two water tanks, two thermal baths, a water pump, a flow meter, a differential pressure sensor, several temperature sensors, valves and pipes. A schematic diagram of the experiment unit is shown in Fig. 5.

The water tanks are used to pump hot or cold water into the test section. Each water tank temperature is controlled by a thermal bath by means of a coiled pipe. These tanks are linked to the test section through valves and pipes, as shown in Figs. 5 and 6.

The water mass flow rate is measured by a Coriolis mass flow meter with

an accuracy of ±0.041 % of the actual flow rate within the operating range. The in-tube water inlet and outlet temperatures are measured with K-type thermocouples with an accuracy of ±0.3 °C. The water pressure drop is obtained from a differential pressure transducer with an accuracy of ±0.04 % F.S.

The Agilent 34970A data acquisition and control module was used coupled with a LabView data logging and control software application.

The experiments were performed in a climatic chamber in order to control the environmental conditions: the temperature of the chamber was kept constant during the experiments. In addition, all the elements of the experimental facility such as tanks and pipes have been fully insulated to reduce heat losses. A commercial insulation has been used (25 mm insulation thickness) for this purpose.

3.1. Test Section

The test section is a drain water heat recovery storage device that consists of a tank with a coiled pipe inside it. The tank is filled with hot water used to store heat while the coiled pipe is used to absorb this energy by means of cold water flowing through it. Fig. 7 shows the instrumented test section, the thermocouples position and its placement in the experimental unit.

The tested tank is cylindrical, the height and the diameter are 350 mm and 250 mm, respectively, and its storage capacity is 15.72 l. It is made of stainless steel and covered with an insulation layer. Eleven calibrated K-type thermocouples with an accuracy of ±0.3 °C are placed inside the accumulator in order to measure the water temperature at different radii and heights. The coiled pipe is made of cooper with a defined external and internal diameter of 15.87 mm and 14.27 mm, respectively. The tube pitch is 25.44 mm. Three calibrated K-type thermocouples (accuracy of ±0.3 °C) are located at the beginning, middle and end of the pipe surface. The inlet tube to the test section is 1.1 m length with an internal diameter of 14.27 mm and a thickness of 1.6 mm. The length of the outlet tube of the test section is 900 mm with the same internal diameter and wall thickness to the inlet tube. These tubes are covered with a commercial insulation layer (20 mm insulation thickness).

3.2. Experimental Procedure

During the operation time of this DWHR storage device three steps take place: the accumulator fluid charge, energy storage and the heat extraction process. In the charging process the tank is filled with hot water coming from

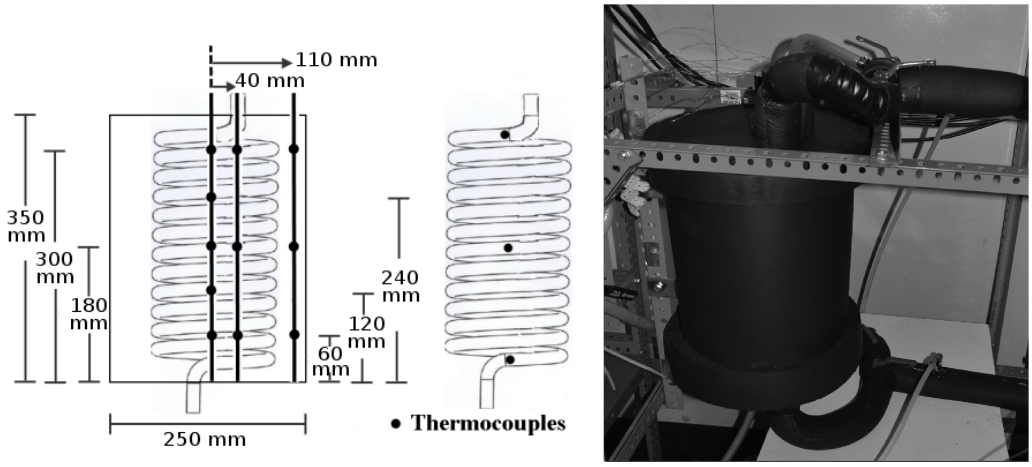

Figure 7: On the left test section, thermocouples located inside the accumulator at different radii and heights. On the right, instrumented and mounted in the experimental unit.

hot water tank. When the tank is full of water, the storage process begins and it finishes when the extraction (discharging) process starts. Finally, the stored energy is extracted in the discharging process by cold water pumped through the accumulator coiled pipe. At this point, all the operational steps are completed.

An uncertainty analysis has been applied to evaluate the errors influence of the different variables measured on the experimental results, which is based on a propagation error methodology proposed in the technical literature [42, 43]. The maximum uncertainty estimated for the heat transfer rate is around ± 11.98 %, while ± 7.88 % was obtained as a maximum uncertainty for the energy recovered during the thermal extraction process.

4. Results

The performance of a DWHR storage device is characterized by different parameters such as the storage capacity, the heat transfer rates during charging and discharging and the storage efficiency.

The authors consider that for both the experimental and numerical tests carried out, the heat extraction and the storage processes are the most relevant steps to be analysed. The charging process is less critical for the design of this type of DWHR (it mainly depends on the filling water amount and temperature).

The non-dimensional temperature shown in the results is calculated as $T^*=(T - T_{min})/(T_{max}-T_{min})$, where T_{min} is the minimum temperature of the water flow through the coiled pipe, T_{max} the initial maximum temperature of the water inside the accumulator in every test condition of the DWHR.

4.1. Test Conditions

The experiments and the numerical simulations for the discharging process are conducted for three different flow rates through the coil and for two different values of initial water temperature at the in-tank (60 °C and 34 °C) defined as high (HT) and intermediate (MT) temperatures, respectively. The in-tube cold water is about 15 °C. Parameters tested in this study are shown in Table 1. The inlet and the outlet tubes has been taking into account in the simulations.

Table 1: Test conditions.

Test	Flow rate [l/min]	$Tini_{in-tank}{}^*$	$Tini_{in-tube}{}^*$	$V_{in-tank}$ [l]	$V_{extractionProcess}$ [l]
1	3				
2	6	1.0 (MT)			
3	9				
4	3		0.0	15.72	20
5	6	1.0 (HT)			
6	9				

And additional experimental test have been carried out to study the heat loss to the environment during the storage period of the DWHR storage device. In this test, the initial water temperature at the in-tank was the high temperature (HT). The fluid flow through the coiled pipe in tests 1 and 4 are in a laminar flow regime, while for the remaining tests (2,3,5 and 6) are in the transition region.

4.2. Mesh refinement studies and Boundary Conditions used in the numerical simulations

The DWHR storage device analysed numerically consists of a tank full of high-temperature water and a coiled pipe through which low-temperature water circulates absorbing the energy of the water contained in the tank. The device dimensions have been defined previously in the section 3.1.

In order to evaluate the adequacy of the spatial discretisation, computations have been performed on different meshes. Extensive mesh refinement

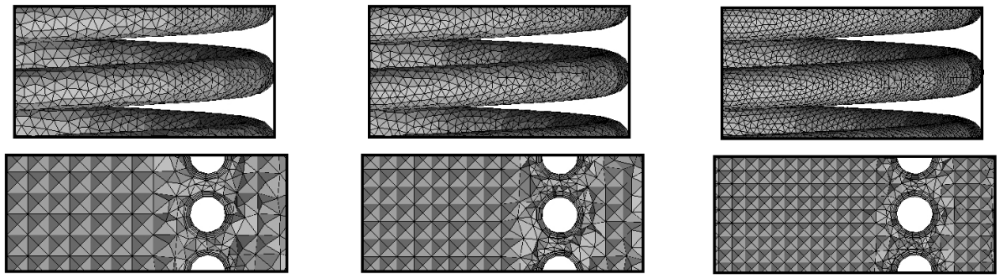

Figure 8: Comparison of the unstructured meshes used for the fluid inside the tank: (left) mesh I; (centre) mesh II; (right) mesh III.

tests have been conducted. A fine near wall mesh is necessary to correctly solve the boundary layer and the physical phenomena associated with the coiled pipe wall. Thus, a prism layer is appropriate in this area due to the low non-orthogonal corrections required by this type of elements.

Three different unstructured meshes are generated attaining the aforementioned criteria to carry out extensive mesh refinement studies. The finest and the coarsest meshes have about 2.0 and 0.68 million elements, respectively. All the meshes guarantee sufficient CVs within the boundary layers, an a priori estimate of the boundary layer has shown that for the studied mean Prandtl number, the thermal boundary layer is thinner than the viscous one as $\delta_t \sim H/Ra^{0.25}$ and $\delta_v \sim Pr^{0.25}\delta_t$ [44]. Details of the tested meshes are shown in Fig. 8.

To sum up, we are not presenting the results obtained with the coarsest and the finest meshes in this paper. However, a thorough comparison of the main parameters of the DWHR storage has been carried out using Test 1. Comparisons have shown good agreement for meshes II and III resulting in, for example, relative differences of as low as 1.2% and 2.2% for the outlet temperature of the in-tube water at the final instant and the energy recovered for the DWHR storage device, respectively. Considering these two meshes, the results are in fairly good agreement with the experiment, even though mesh II (this mesh has about 1.0 million elements (Fig. 9)) is twice as coarse as mesh III. Mesh II has been selected in this work, because the computational time factor was reduced twice and within acceptable results.

The coiled pipe is discretised with a Cartesian grid of 268 x 4 control volumes and the internal fluid flowing through it has 268 control volumes.

The boundary conditions for the fluid inside the tank have been considered with and without heat losses at the tops and sides of the tank during

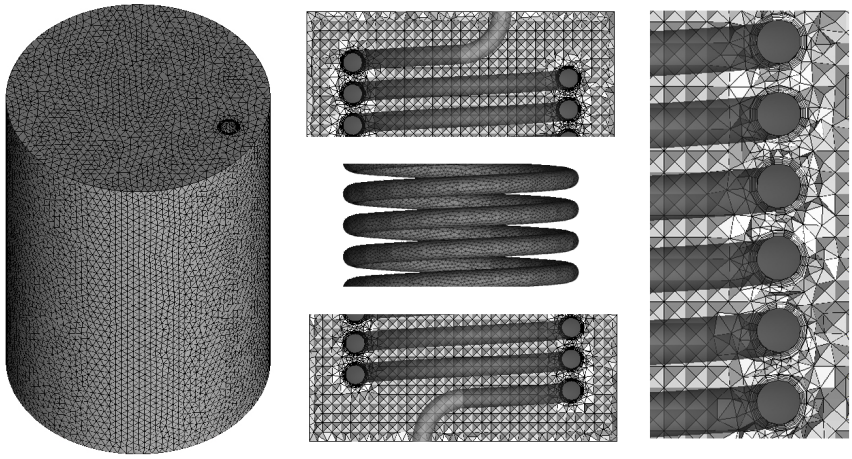

Figure 9: Views of the unstructured mesh used for the fluid inside the tank.

the extraction process. These conditions have been compared using the Test 1 and 4 (with the longest time tests). The results with and without considering the heat losses are highly similar, this is because the heat loss during the extraction process tests are less than 0.1% of the total energy contained in the tank. For this reason, the boundary conditions for the fluid inside the tank are considered adiabatic. And the boundary condition for the fluid flow inside the pipe are: temperature inlet (T_{in}), mass flow inlet ($\dot{m}_{in}$), and pressure inlet (P_{in}), values obtained from the experiments.

4.3. Extraction Process results

For the heat extraction process, both the storage temperature and the water flow rate inside the coiled pipe were studied experimentally and numerically as having a large effect on the extraction energy rate. For each initial temperature (HT and MT), the water flow rate in the coil were 3, 6 and 9 l/min.

A comparison between the numerical and experimental results has been carried out for the different flow rates and temperatures considered. Fig. 10 shows the evolution of the outlet non-dimensional temperature of the in-tube water for the different tests. In general, good agreement can be appreciated between experimental data and numerical results. The numerical results follow the transient evolution of the temperature correctly, although with small differences between them. The results for the final instant show that all the compared test remain within an relative error below 4.8%

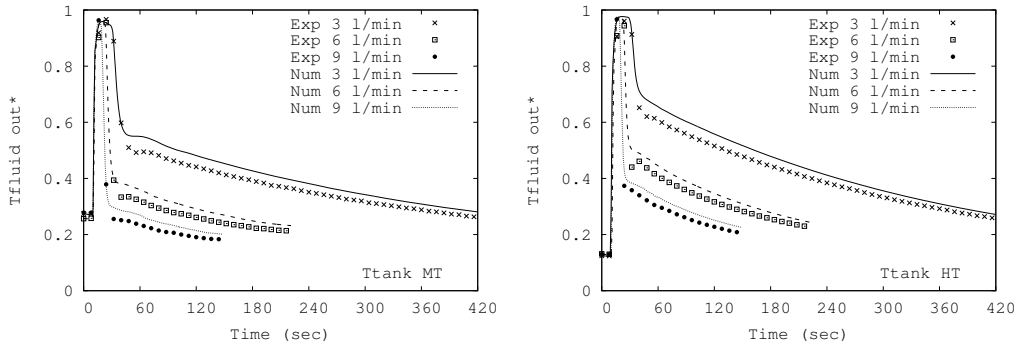

Figure 10: Extraction process: comparison between the numerical simulation and the experiments of the outlet non-dimensional temperature of the in-tube water for different flow rates for in-tank water with: (left) intermediate temperature; (right) high temperature.

(err = 100abs(($T^*_{outletExp}$-$T^*_{outletNum}$)/$T^*_{outletExp}$)[%]). These differences may due to the numerical implementation: use of empirical correlations to solve the in-tube fluid, the numerical schemes and turbulent model used for the in-tank fluid. On the other hand, the assumption that the temperature does not vary in the angular direction of the coiled pipe (solved in 2D way), and the initial conditions (estimated from experimental data) could also have an impact on the numerical prediction. Finally, the experimental uncertainty should also be considered. The peak observed in the different tests is due to the water which is initially contained within the coiled pipe and is hotter than the water entering it. These results revealed that the rise in the temperature of the fluid was significantly affected by the flow rate reduction. This effect is caused because the heat transfer rate rises by a smaller proportion than the flow rate.

Experimental and numerical results of the in-tank water non-dimensional temperature along the height of the tank for the all tests are shown in Fig. 11. It can be observed that the water temperature at the final instant is decreasing with more intensity in the bottom part of the tank, because the inlet of the cold water in-tube is located in that area of the tank. The numerical results followed a trend similar to the experimental data for the different flow rates. Furthermore, it can be seen the influence of the flow rates on the temperature distribution. Fig. 11 also shows that in the lower part of the tank the measured values are modelled quite accurately. However, the measured values in the upper sensor (h= 300 mm) show distinctly higher deviations between experiment and simulation. The authors believe that the

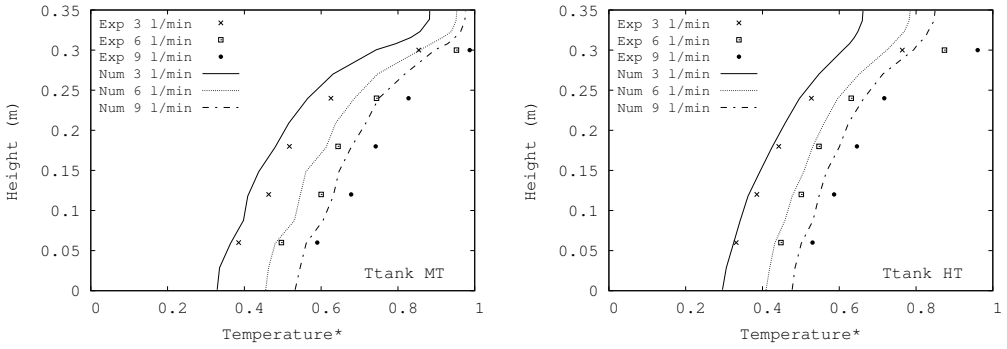

Figure 11: Extraction process: comparison between the numerical simulation and the experiments of the non-dimensional temperature of the in-tank water at the final instant. On the left, tests with intermediate temperature. On the right, tests with high temperature.

discrepancies in the in-tank water in height ≤ 250 mm are considered to be due to the aspects mentioned above for Fig. 10. For height ≥ 300 mm, a local effect of under prediction of temperature in the numerical side is observed. This deviation is probably caused by the boundary condition assumed in the tank walls, as in reality the thermal inertia will create experimentally transient heating effect in this zone. Here this effect is more relevant because the coiled pipe surface is very small (vertical outlet).

Another interesting variable to show in the extraction process is the percentage of energy recovered for the DWHR storage device for the different flow rates and temperatures considered (Fig. 12). The heat transfer rate was calculated based on the mass flow rate, $\dot{m}$, the specific heat of the in-tube fluid, c_p, and the difference in inlet and outlet temperatures ($T_{out} - T_{in}$).

The total energy delivered by the in-tank water is the integration of the heat transfer rate during the test. The total energy recovered or delivered is made dimensionless by dividing by the total energy contained in the in-tank water at the initial time test with respect to the minimum inlet temperature of the in-tube water. It is shown that the in-tube flow rate is the dominating parameter.

Detailed comparisons between the experimental and numerical results for Test 1 (MT, 3 l/min) are shown below. Figs. 13 (left), 13 (right) and 14 (left) show the evolution of the non-dimensional temperature over time at different locations inside the accumulator in the DWHR storage device. The greater effect of the height on the temperature can be clearly seen, while smaller effect was determined in the radial direction. A reasonable agreement can

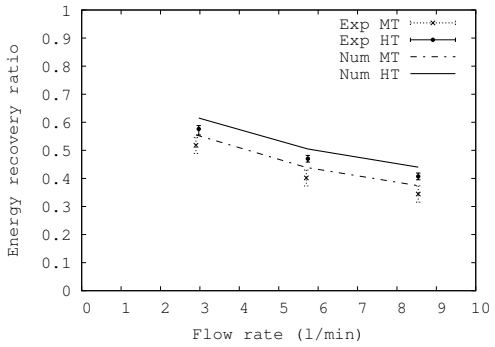

Figure 12: Heat extraction process: comparison between the numerical simulation and the experiments of the energy recovery ratio for different flow rates.

be appreciated between experiment and numerical simulation. However, discrepancies have been found in the temperature of the in-tank water located at a height of 300 mm. As explained above, the authors believe this may be due to the thermal inertia of the tank walls will generate experimentally a transient heating effect in this zone.Two extra sensors have been added numerically at heights of 305 and 310 mm to appreciate the transient behaviour of the DWHR storage in this zone.

The non-dimensional temperature of the in-tube water along the time at different positions are shown in Fig. 14 (right). Fig. 14 (right) shows that the rise of temperature is reduced over time due to the cooling process in the in-tank water. Furthermore, Fig. 14 (right) shows a good agreement between the numerical simulations and experiments. The numerical simulations performed seem to reasonably predict the transient behaviour of the in-tube water.

Fig. 15 (left) shows the profile along the time of the heat transfer rate from the in-tank water to the in-tube water. As would be expected, the profile of the heat transfer rate has the same behaviour as the outlet temperature of the in-tube water. The evolution over time of the total energy delivery ratio by the DWHR storage device as shown in Fig. 15 (right).

For the case studied, the numerical results and measured results show a high degree of correspondence. Good agreement was also attained for the heat transfer rate and the total energy delivery ratio. However, small discrepancies were identified in the non-dimensional temperature over time at height 300 mm inside the accumulator. Regarding the in-tube water, the numerical results show an acceptable agreement with the experimental data

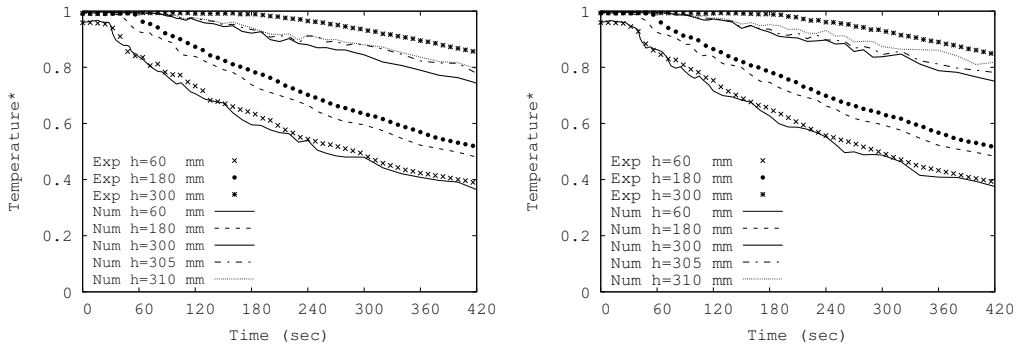

Figure 13: Test 1: Transient evolution of non-dimensional temperature of the in-tank water at different positions: (left) r= 0. (right) r= 40 mm.

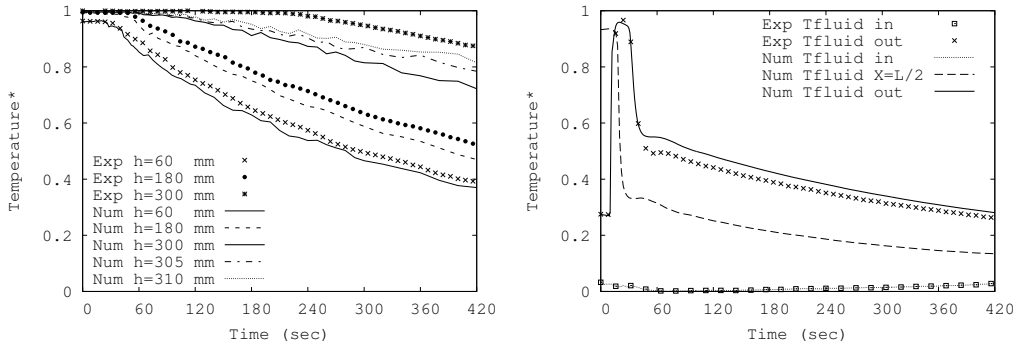

Figure 14: Test 1: Transient evolution of non-dimensional temperature of: (left) the in-tank water at r= 110 mm. (right) the in-tube water at different positions.

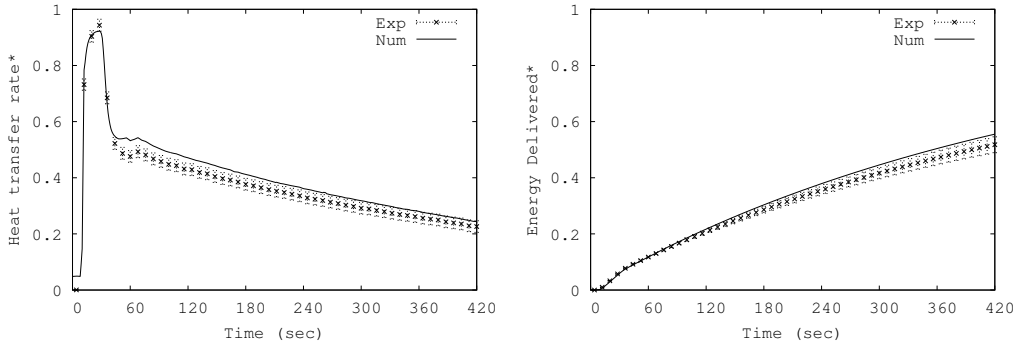

Figure 15: Test 1: Transient evolution of: (left) non-dimensional heat transfer rate; (right) the energy delivery ratio of the device.

in the DWHR storage during the extraction process.

The numerical model provides additional and more detailed information of the heat extraction process at any time of the natural movement of the water and the temperature distribution inside the DWHR storage. Figs. 16 and 17 show the 3D streamline and the transient evolution of the non-dimensional temperature of the water in the tank, respectively, for Test 1. The cooled tank water near the coiled pipe wall travels down and moves through the tubes forming streams which advance towards the bottom of the tank. These streams of cooled water interact continuously with the water in the core. When the streams in the bottom arrive to the centre and to the lateral wall of the tank, upward streams are formed as shown in Fig. 16, and in greater detail at 60 seconds in Fig. 17. As the interaction between the cooled water on the coiled pipe wall and the water in the core continues, the stratification of the fluid temperatures advances from the bottom to the top, see Fig 16. Furthermore, it is seen how the in-tank water temperature decreases progressively from bottom to top of the tank getting closer to the in-tube inlet temperature, due to the energy delivery process to the in-tube water.

The average outer Nusselt number ($\overline{Nu_o}$) is defined in this problem as a function of the fluid (in-tank) and the wall (coiled pipe) temperatures. The Nusselt number is numerically calculated in this work and can be defined as:

$$\overline{Nu_o} = \frac{L_{ref}}{\Delta T_{ref} S} \int_S \frac{\partial T}{\partial n} ds \tag{19}$$

where, ΔT_{ref} =($T_{in-tank,t=0}$ - $T_{in-tube,inlet}$), L_{ref} is the characteristic length, and S is the outer surface of coiled pipe. For this work the coil height is taken as characteristic length.

Fig. 18 shows the evolution of the average outer Nusselt number for intermediate temperature (MT) and flow rates of 3 l/min (left) and 9 l/min (right). The Nusselt number behaviour is described by means of a curve divided into two zones. Zones 1 corresponds to the initial evolution of the Nusselt number, increasing until it reaches a maximum value. At first, there is a strong increase in the temperature difference between the wall and the in-tank water promoted by the inlet in-tube water. While in zone 2, the Nusselt number decreases at a constant rate with time as the difference between the in-tank water and the wall temperature decreases. It is also observed that the Nusselt number increases with the flow rate.

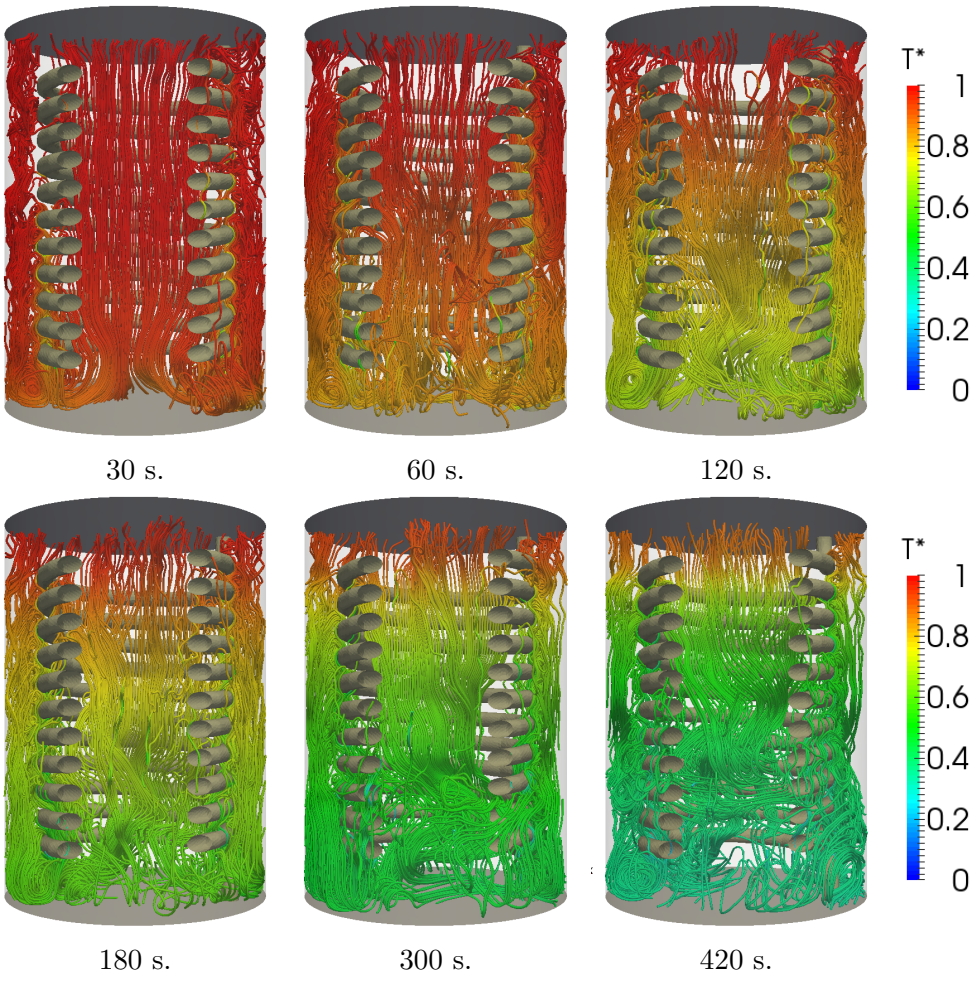

Figure 16: Test 1: in-tank water 3D streamline for different instants of time (s).

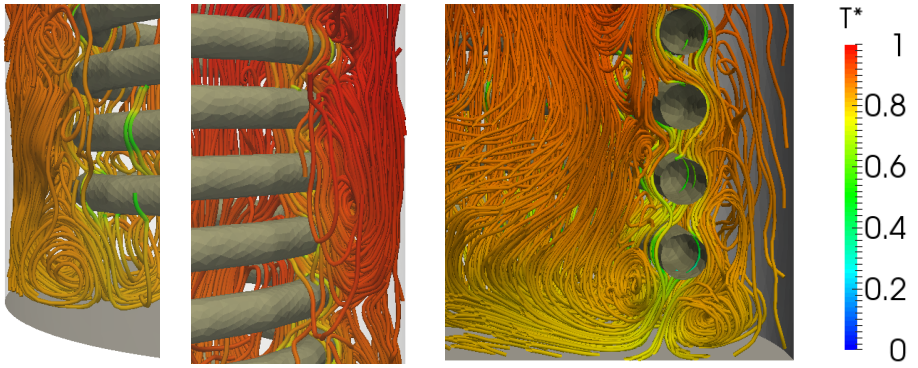

Figure 17: Test 1: in-tank water 3D streamline detail at 60 seconds.

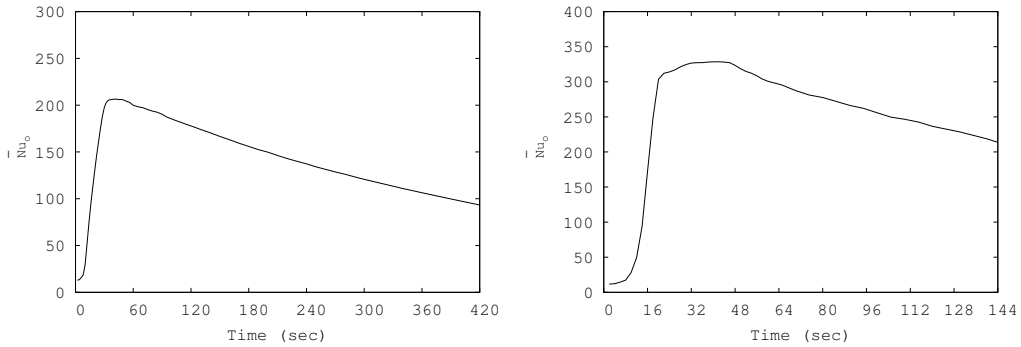

Figure 18: Evolution of the overall outer Nusselt number for intermediate temperature (MT) and flow rates: (left) 3 l/min and (right) 9 l/min.

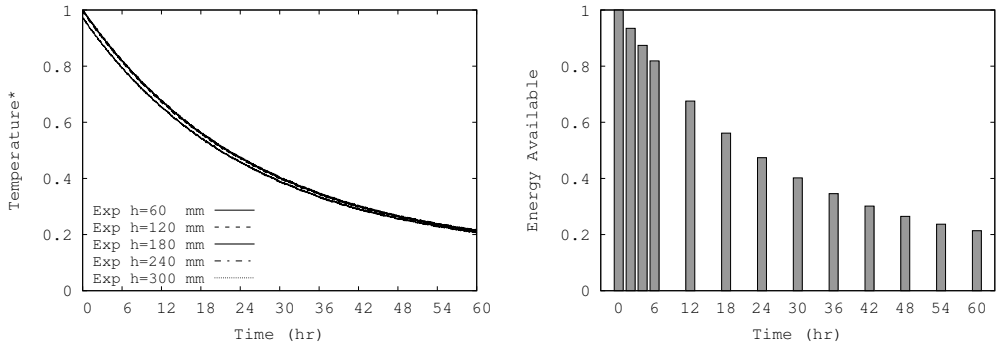

Figure 19: Storage process: on the left, evolution of non-dimensional temperature of the in-tank water at different positions in r=0. On the right, available energy in the DWHR storage device with time.

4.4. Storage Process results

For storage process a test of heat loss to the environment of the DWHR storage device has been carried out experimentally, considering an initial non-dimensional temperature of 1.0 (HT) for the water inside the tank. The test was performed in a climatic chamber, where its non-dimensional temperature was kept constant during the experimental test at 0.11. The duration of the heat loss test was 60 hours.

In Fig. 19 (left) the vertical non-dimensional temperature measurements of the in-tank water are plotted over the duration of the test. These results show that the bottom of the storage dropped in temperature little more than the other temperature sensors located directly above. An exponential decay of the water temperature inside the tank during the test period was observed. It was also noted that there were no significant temperature gradients in the radial direction. Additionally, the available energy in the DWHR storage device with time has been obtained from the experimental data Fig. 19 (right). This available energy is calculated with respect to the initial instant and for use in the extraction process with cold water. The DWHR storage device has been insulated with a 25 mm closed cell elastomeric insulation layer (λ=0.04 W/m.K). A 50% reduction in stored energy is observed at 24 h, which reveals its limitations for long-term storage applicability.

5. Conclusions

A specific drain water heat recovery storage-type based on a cylindrical tank with an internal coiled pipe has been built. In this work both numerical and experimental tools have been used to design and study the performance of this device.

The experimental unit provides reliable measurements of the temperatures at different locations (in-tank and in-tube) and the flow rate, to study the storage capacity and the delivering energy process of the DWHR storage device. The experiments have generated the required data for the boundary conditions definition and results for validation of the numerical simulations.

A numerical simulation platform has been adapted for the prediction of the DWHR storage system, providing additional and more detailed information. The in-tank water natural convection flow and its local temperature evolution are described by a 3D transient CFD analysis.

Extraction process tests were conducted to determine the effect of flow rate and temperature in the heat recovery performance of the DWHR storage device. For the DWHR storage built in this work, the maximum heat recovered is reached at the lowest flow rates (3 l/min) for the two different in-tank temperatures. The DWHR storage had the capacity to recover from 34% - 60% of the energy available in the drain water for the investigated flow rates. In these tests a comparison between the numerical and experimental results has been carried out. Different results of the DWHR storage device are shown, such as the evolution of the non-dimensional temperature over time of the water in-tank and in-tube and the energy recovery ratio, where the numerical results were shown a trend similar to the experimental data for the different tests.

A heat losses test was also conducted. There were no significant temperature gradients in the radial direction. A 50% reduction in stored energy is observed at 24 h, which reveals its limitations for long-term storage applicability.

The objective of these devices is the recovery of the waste heat from domestic warm drain water and transferring it to cold water entering the house. From the results, it can be concluded that the objective has been reached with the proposed design.

Nomenclature

$\mathbf{C}$	Convective operator
c_p	specific heat capacity
$\mathbf{D}$	Diffusive operator
D	diameter of curvature
d	tube diameter
De	Dean number
e	energy
f	friction factor
$\mathbf{G}$	Gradient operator
g	gravity
h	enthalpy
L	length
$\mathbf{M}$	Divergence operator
m	mass
$\dot{m}$	mass flow rate
Nu	Nusselt number
p	pressure, pitch
Pr	Prandtl number
$\dot{Q}$	heat transfer
r	radial direction, radius
Re	Reynolds number
S	surface area
T	temperature
t	time
u, $\mathbf{u}$	velocity magnitude, velocity vector
V	volume
v, $\bar{v}$	velocity magnitude, mean velocity
z	axial coordinate

Greek symbols

α	heat transfer coefficient
β	thermal expansion coefficient
δ_t	thermal boundary layer
Δ_r	radial step
Δ_z	axial step
θ	angle to gravity
λ	thermal conductivity
μ	dynamic viscosity
ν	kinematic viscosity
Ω	Matrix with the volumes of the cells
ρ	density
τ	shear stress

Superscripts and subscripts

c	kinetic
cri	critical
E	east node
e	control volume east face
Exp	referred to the experiment
in	inlet
$in-tank$	referred to the fluid inside the tank
$in-tube$	referred to the fluid inside the tube
N	north node
n	control volume north face
Num	referred to the numerical simulation
out	outlet
p	potential, current node
ref	characteristic
S	south node
s	control volume south face
$tube$	referred to the tube
vms	variational multiscale
W	west node
w	control volume west face
$wall$	referred to wall
0	initial time

Abbreviations

CFD	computational fluid dynamic
CFL	Courant Friedrichs Lewy
CV	number of control volumes
DNS	direct numerical simulation
$DWHR$	drain water heat recovery
HT	heat transfer, high temperature
MT	intermediate temperature
LES	large eddy simulation
$RANS$	Reynolds Averaged Navier Stokes
SWH	solar water heating
VMS	variational multiscale
$WALE$	wall-adapting local eddy-viscosity

Acknowledgments

This work has been financially supported by the Ministerio de Economía y Competitividad, Secretaría de Estado de Investigación, Desarrollo e Innovación, Spain (CEN-20091005), by the project SEILA New technologies for an efficient, ecologic and intelligent washing system for textiles of the future (Ref. C07973).

References

[1] DOE, 2011 buildings energy data book, U.S. Department of Energy, 2011.

[2] Energy Consumption in the UK (2014), Department of Energy & Climate Change, London SW1A 2AW. www.gov.uk/decc.

[3] P.J. Boait, D. Dixon, D. Fan, A. Stafford, Production efficiency of hot water for domestic use, Energ. Buildings 54 (2012) 160–168.

[4] C.M. Leidl, W.D. Lubitz, Comparing domestic water heating technologies, Technol. Soc. 31 (2009) 244–256.

[5] A. Cooperman, J. Dieckmann, J. Brodrick, Drain Water Heat Recovery, ASHRAE Journal 2011 (2011).

[6] C. Zaloum, M. Lafrance, J. Gusdorf, Drain water heat recovery characterization and modeling, Final draft, Sustainable Building and Communities, Natural resources, Canada (2007).

[7] A. McNabola, K. Shields, Efficient drain water heat recovery in horizontal domestic shower drains, Energ. Buildings 59 (2013) 44–49.

[8] L.T. Wong, K.W. Mui, Y. Guan, Shower water heat recovery in high-rise residential buildings of Hong Kong, Appl. Energ. 87 (2010) 703–709.

[9] X. Liu, L. Ni, S.K. Lau, H. Li, Performance analysis of a multi-functional Heat pump system in heating mode, Appl. Therm. Eng. 51 (2013) 698–710.

[10] W. Chen, S. Liang, Y. Gou, K. Cheng, Investigation on the thermal performance and optimization of a heat pump water heater assisted by shower waste water, Energ. Buildings 64 (2013) 172–181.

[11] J. Wallin, J. Claesson, Investigating the efficiency of a vertical inline drain water heat recovery heat exchanger in a system boosted with a heat pump, Energ. Buildings 80 (2014) 7–16.

[12] L. Ni, S.K. Lau, H. Li, T. Zhang, J.S. Stansbury, J. Shi, J. Neal, Feasibility study of a localized residential grey water energy-recovery system, Appl. Therm. Eng. 39 (2012) 53–62.

[13] D.G. Prabhanjan, G.S.V. Raghavan, T.J. Rennie, Comparison of the heat transfer rates between a straight tube heat exchanger and helically coiled heat exchanger, Int. Commun. Heat Mass 29 (2) (2002) 185–191.

[14] W.R. Dean, Note on the motion of fluid in a curved pipe, Philos. Mag. 4 (1927) 208–223.

[15] W.R. Dean, The stream-line motion of fluid in a curved pipe, Philos. Mag. 5 (1928) 673–695.

[16] H. Ito, Friction factors for turbulent flow in curved pipes, Trans. Amer. Soc. Mech. Eng. J. 81 (1959) 123–132.

[17] R. Seban, E.F. McLaughlin, Heat transfer in tube coils with laminar and turbulent flow, Int. J. Heat Mass Transfer 6 (1963) 387–395.

[18] G. F. Rogers, Y.R. Mayhew, Heat transfer and pressure loss in helically coiled tubes with turbulent flow, Int. J. Heat Mass Transfer 7 (1964) 1207–1216.

[19] E.F. Schmidt, Wärmeübergang und nicht isothermer Druckverlust bei erzwungener Strömung in schraubenförming gekrümmten Rohren, Dr. -Ing. Diss. TH Braunschweig, F.R.G. (1966).

[20] V. Gnielinski, Heat transfer and pressure drop in helically coiled tubes, In: Proceeding 8th Int. Heat Transfer Conference 6 (1986) 2847–2854.

[21] E.F. Schmidt, Wärmeübergang und Druckverlust in Rohrschlangen, Chem. Ing. Tech. 39 (1967) 781-789.

[22] A.N. Dravid, K.A. Smith, E.W. Merrill, P.L.T. Brian, Effect of secondary fluid motion on laminar flow heat transfer in helically coiled tubes, AIChE J. 17 (1971) 1114–1122.

[23] M.E. Ali, Experimental investigation of natural convection from vertical coiled tubes, Int. J. Heat Mass Transfer 37 (1994) 665–671.

[24] M.E. Ali, Free convection heat transfer from the outer surface of vertically oriented helical coils in glycerol-water solution, Heat Mass Transfer 40 (2004) 615–620.

[25] R.C. Xin, M.A. Ebadian, Natural convection heat transfer from helicoidal pipes, J. Thermophys. Heat Tr. 10 (1996) 297–302.

[26] R.C. Xin, M.A. Ebadian, The effects of Prandtl numbers on local and average convective heat transfer characteristics in helical pipes, J. Heat Transf. 119 (1997) 467–473.

[27] D.G. Prabhanjan, T.J. Rennie, G.S.V. Raghavan, Natural convection heat transfer from helical coil tubes, Int. J. Therm. Sci. 43 (2004) 615–620.

[28] J. Fernández-Seara, C. Piñeiro-Pontevedra, J.A. Dopazo, On the performance of a vertical helical coil heat exchanger. Numerical model and experimental validation, Appl. Therm. Eng. 62 (2014) 680–689.

[29] J. Lopez, O. Lehmkuhl, R. Damle, J. Rigola, A parallel and object-oriented general purpose code for simulation of multiphysics and multi-scale systems, In: Proceedings of the 24th International Conference on Parallel Computational Fluid Dynamics, 2012.

[30] R. Damle, O. Lehmkuhl, G. Colomer, I. Rodríguez, Energy simulation of buildings with a modular object-oriented tool, In: Proceedings of the ISES World Conference, 2011.

[31] O. Lehmkuhl, C.D. Pérez-Segarra, R. Borrell, M. Soria, A. Oliva, TERMOFLUIDS: A new Parallel unstructured CFD code for the simulation of turbulent industrial problems on low cost PC Cluster, In: Proceedings of the Parallel CFD 2007 Conference, 2007.

[32] S. Morales-Ruiz, J. Rigola, C.D Pérez-Segarra and O. García-Valladares, Numerical analysis of two-phase flow in condensers and evaporators with special emphasis on single-phase/two-phase transition zones, Appl. Therm. Eng. 29 (2009) 1032–1042.

[33] A.J. Chorin, On the convergence of discrete approximations to the Navier-Stokes equations, Math Comput. 23 (1969) 341–353.

[34] R. Temam, Navier-Stokes Equations. Theory and Numerical Analysis, 2nd ed., North-Holland, Amsterdam, 1979.

[35] R.W.C.P. Verstappen, A.E.P. Veldman, Symmetry-preserving discretization of turbulent flow, J. Comput. Phys. 187 (2003) 343–368.

[36] T.J.R. Hughes, L. Mazzei, K.E. Jansen, Large eddy simulation and the variational multiscale method, Comput. Vis. Sci. 3 (2000) 47–59.

[37] O. Lehmkuhl, I. Rodríguez, A. Baez, A. Oliva, C.D. Pérez-Segarra, On the large-eddy simulations for the flow around aerodynamic profiles using unstructured grids, Comput. Fluids 84 (2013) 176–189.

[38] D.E. Aljure, O. Lehmkuhl, I. Rodríguez, A. Oliva, Flow and turbulent structures around simplified car models, Comput. Fluids 96 (2014) 122–135.

[39] S. Torras, O. Lehmkuhl, J. Rigola, A. Oliva, Numerical simulation of heat storage for domestic applications, In: Proceedings of the 23rd IIR Int. Congress of Refrigeration, 2011.

[40] V. Gnielinski, Zur Berechnung des Druckverlustes in Rohrwendeln, Vt-Verfahrenstechnik 17 (1983) 683–690.

[41] G. Woschni, Untersuchung des Wärmeübergangs und des Druckverlusts in gekrümmten Rohren, Dr. -Ing. Diss. Universität Karlsruhe, F.R.G. (1985).

[42] R. J. Moffat, Describing the uncertainties in experimental results, Exp. Therm. Fluid Sci. 1 (1998) 3–17.

[43] H. W. Coleman, W. G. Steele, Experimentation and uncertainty analysis for engineers, John Wiley and Sons, Inc. New York, 1998.

[44] D. Kizildag, I. Rodríguez, A. Oliva, O. Lehmkuhl, Limits of the Oberbeck-Boussinesq approximation in a tall differentially heated cavity filled with water, Int. J. Heat Mass Transfer 68 (2014) 489–499.